Interpolating Wavelets and Adaptive Finite Difference Schemes for Solving Maxwell's Equations: The Effects of Gridding

Pedro Pinho[1], Margarete O. Domingues[2], Paulo J. S. G. Ferreira[3], Sônia M. Gomes[4], Anamaria Gomide[5], and José R. Pereira[6]

[1]Instituto Superior de Engenharia de Lisboa, DEETC/IT, Lisboa 1950-062, Portugal
[2]Instituto Nacional de Pesquisas Espaciais, LAC, São José dos Campos SP 12245-970, Brazil
[3]Universidade de Aveiro, DETI/IEETA, Campus Universitário de Santiago, Aveiro 3810-193, Portugal
[4]Universidade Estadual de Campinas, IMECC, Campinas SP 13083-970, Brazil
[5]Universidade Estadual de Campinas, IC, Campinas SP 130874-971, Brazil
[6]Universidade de Aveiro, DETI/IT, Campus Universitário de Santiago, Aveiro 3810-193, Portugal

In this paper, we discuss the use of the sparse point representation (SPR) methodology for adaptive finite-difference simulations in computational eletromagnetics. The principle of the SPR method is to represent the solution only through those point values indicated by the significant wavelet coefficients, which are used as local regularity indicators. Recently, two kinds of SPR schemes have been considered for solving Maxwell's equations: 1) staggered grids in the time-space domain are used for the discretization of the magnetic and electrical fields, as in the finite-differences time-domain (FDTD) scheme and 2) nonstaggered grids are used in combination with Runge-Kutta ODE solvers. In both cases, 1-D simulations of the SPR method leads to sparse grids that adapt in space to the local smoothness of the fields, and, at the same time, track the evolution of the fields over time with substantial gain in memory and computational speed. However, in the latter case, we found spurious oscillations in the simulations. Therefore, before extending the implementation of the SPR method to higher dimensions, we wanted to evaluate which of these two SPR strategies is more convenient. After a careful theoretical analysis of stability and numerical dispersion comparing the schemes in staggered and nonstaggered grids, we conclude that schemes for staggered grids seem to be preferable from the dispersion viewpoint, especially for low-order schemes and coarse grids. However, by adapting the grid density and increasing the order, SPR schemes for nonstaggered grids also show good performance. In our experiments, no spurious oscillations were detected. We observed that, for a given accuracy, the adaptive scheme on a nonstaggered grid requires less computational effort. Since the use of nonstaggered grids increases the stability range and facilitates the implementation of adaptive strategies, we believe that the SPR method in nonstaggered grids has a very good potential for computational electromagnetics.

Index Terms—**Interpolating wavelets, multiresolution, numerical dispersion, numerical stability, sparse point representation (SPR).**

I. Introduction

COMPUTATIONAL electromagnetics is a very active area, with a rich variety of numerical methods [1]–[5]. One of the most often used is Yee's FDTD scheme. In the FDTD scheme, electric and magnetic fields are described by vectors containing their sample values at staggered grid points, uniformly distributed in the space–time domain, and partial derivatives are approximated by centered finite differences of second order. To improve the performance of the FDTD method, higher order difference schemes may be applied, reducing the number of cells per wavelength required to achieve a certain degree of accuracy, as described in [6]. However, in the presence of local irregularities, the grid density needs to be increased, even for higher order methods. Thus, uniform gridding is not a practical option, since oversampling may occur in regions of smoothness. For numerical simulation of irregular solutions of partial differential equations, significant improvements in accuracy and computational efficiency may be obtained by adapting the grid points to the numerical solution.

In the wavelet context, the multiresolution time-domain technique (MRTD) [7] offers a natural framework for the definition of dynamic adaptive strategies for Maxwell equations. The MRTD method is a Galerkin scheme, and there are two equivalent versions, depending on the choice of the basis for the test functions. The one-scale-level version S-MRTD uses scaling functions and works as higher order finite difference schemes on uniform grids. The W-MRTD version uses wavelets in a multilevel setting and adaptability is obtained by thresholding small wavelet contributions. In the S-MRTD version, these MRTD methods tend to improve the numerical dispersion effect, in certain circumstances of the CFL (Courant–Friedrics–Lewy) parameter, allowing a cutting down of the computational requirements. However, for the multilevel wavelet version W-MRTD, the implementation complexity increases with the number of scale levels, seriously compromising the computational performance.

There is another type of adaptive strategy called sparse point representation (SPR) that uses interpolating wavelets tools [8], [9]. The principle of the method is to represent the solution only through those point values indicated by the significant wavelet coefficients, which are defined as interpolation errors. Typically, few points are needed in each time step, the grid

Digital Object Identifier 10.1109/TMAG.2006.889050

being coarse in smooth regions, and refined close to irregularities. The method has two basic parts. In the representation part, there are wavelet tools containing reconstruction operators defined by means of interpolating subdivision schemes. In the operational part, spatial derivatives are discretized by uniform finite differences, using step sizes that can be made proportional to the local scale at each point. It may occur that some required neighboring stencils are not present in the grid. In such case, the corresponding point values are approximated from coarser scales using the wavelet tools of the representation part. Unlike the W-MRTD method, the computation of nonlinear functions (such as products and squares, for example) is easily obtained in the SPR method, since the data are samples of the fields. For the same reasons, enforcing boundary conditions in the SPR scheme is a simple matter.

We believe that the SPR method has a very good potential for computational electromagnetics. For instance, an application of the SPR method adapted to staggered grids is described in [10], [11] for the solution of Maxwell's equations, where 1-D simulations and comparisons with the FDTD scheme are presented. The method leads to sparse grids that adapt in space to the local smoothness of the fields, and, at the same time, track the evolution of the fields over time with substantial gain in memory and computational speed. In [12], another application of the SPR method for the solution of Maxwell's equations using nonstaggered grids, combined with Runge–Kutta ODE solvers, shows that the method is able to describe the propagation updating with a relatively small number of field samples. However, the authors report the occurrence of spurious oscillations in their simulations. Therefore, before extending the implementation of the SPR method to higher dimensions, our purpose here is to evaluate which one of these two SPR strategies is more convenient.

In Section II, we describe the main properties of the SPR method, and in Section V we present results of numerical simulations comparing the two SPR strategies. For this purpose, firstly, in Section III, we describe two classes of finite differences (FD) discretizations for Maxwell's equations that can be used in the operational part of the SPR method. In one class, we consider uniform staggered grids in the time-space domain for the components of magnetic and electrical fields, as in the FDTD scheme. But we shall also consider another class of schemes based on uniform nonstaggered grids. Our goal in Section IV is to compare these two classes of FD schemes with respect to numerical dispersion and stability, since the effects of these properties are very important for the performance of the SPR method. For the sake of clarity in our applications, we shall discuss some examples that can be formulated in a unified way, via the collocation method in approximation spaces defined by the translations and dilations of a basic interpolating function $\Phi(x)$. In particular, we shall analyze in detail some cases taken from the family of Delauriers–Dubuc scaling functions [13], which are the basis for the construction of interpolating multiresolution analyses. However, it should be noted that other finite difference stencils could be used as well, since in the SPR methodology the operational and representation parts may be chosen independently.

With respect to numerical dispersion studies, we take into account the grid density effect and CFL number. It is usual to find articles in the literature comparing the performance of numerical schemes with different stability ranges, where the conclusion of the superiority of one scheme over another is based on the numerical dispersion at a fixed CFL number, for instance, as in [14]. As shown in some illustrative examples of the present paper, there are cases where this kind of conclusion may be unfair, and a more accurate analysis would need to take into account the CFL effect. More precisely, it is important to evaluate and to compare the CFL numbers required for the schemes to achieve a prescribed accuracy level, with a certain number of cells per wavelength.

The conclusions extracted from the theoretical analysis and numerical simulations of the paper are summarized in Section VI. We infer, for example, that the schemes based on staggered grids seem to be preferable from the dispersion view point, specially for low orders and coarse grids, and that they require less computational effort to achieve a certain accuracy. Since the use of nonstaggered grids also increases the stability range, we conclude that they are preferable, and have a very good potential for computational electromagnetics.

The Appendix describes the basic functions used in the approximations and the main definitions about interpolating wavelets.

II. The SPR Method

The SPR method is an adaptive finite difference strategy for evolutive partial differential equations

$$u_t(x,t) = Lu(x,t), \quad t > 0, \quad x \in \Omega$$

augmented with initial and boundary conditions. The method combines the simplicity and accuracy of traditional FD schemes with the ability of wavelet coefficients in the characterization of local regularity of functions. It has two basic parts: the operational part, and the representation part. In the operational part, the background context is that of an accurate and stable FD scheme where the solutions are represented by vectors $U^n = U^{n,j}$ containing approximated node values at points ν in a uniform grid X^j, and time $t^n = n\Delta t$. Namely, $U^n_\nu \approx u(\nu, n\Delta t), \nu \in X^j$. At the next time step, U^{n+1} is obtained by the application of a discrete evolution operator $\mathcal{L} = \mathcal{L}^{j,\Delta t}$, such that $U^{n+1} = \mathcal{L}U^n$. The action of $\mathcal{L}$ includes the discretization of the spatial differential operator L by a FD scheme, the discretization in time by means of some ODE solver, and the enforcement of boundary conditions. In the representation part, there are wavelet tools containing reconstruction operators defined by means of interpolating subdivision schemes. For discretizations of a function on a grid $\Gamma \subset X^j$, the wavelet transform makes use of reconstruction operators, which are defined by means of an interpolating subdivision scheme. The discrete information of a function f at Γ is organized by levels of resolution. At each level l, the wavelet coefficients d^l are defined in terms of local interpolation errors at the new points of the current level of discretization. In the construction of the adapted grids, the idea is to use the wavelet coefficients as indicators of local smoothness of the solution. This is the main ingredient in the definition of the thresholding operator $\mathcal{T}_\varepsilon$: only those points corresponding to wavelet coefficients of magnitude greater than ε should be kept in the adapted grid Γ_ε.

In the adaptive SPR method, the goal consists of performing the FD model in a more economic fashion, by taking into account local regularity information about the numerical solution.

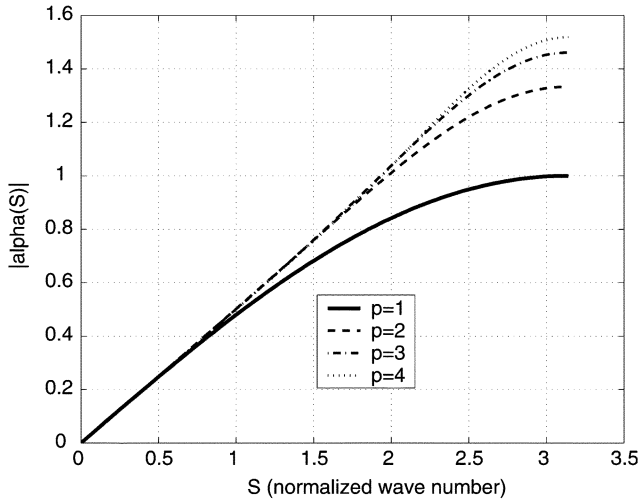

(a)

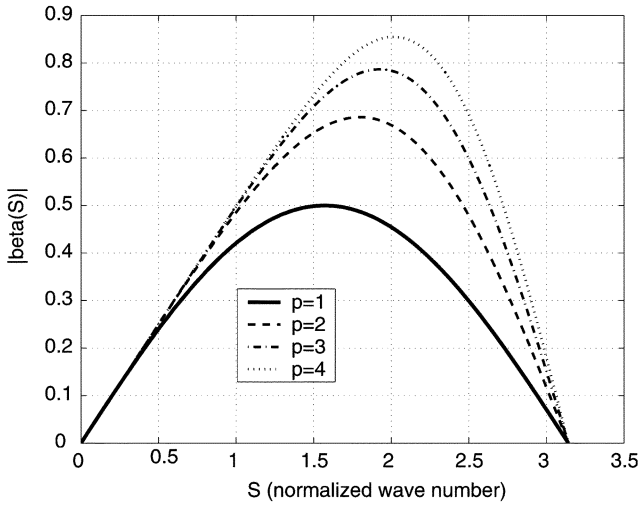

(b)

Fig. 1. Plots of $\bar{\alpha}$ (top, staggered grid) and $\bar{\beta}$ (bottom, nonstaggered grid) versus the normalized wave number S, for different orders p. (a) Staggered grid. (b) Nonstaggered grid.

The first step in this direction is the representation of the numerical solution $U_a^n = U_a^{j,n}$ in a sparse grid $\Gamma^n = \Gamma^{j,n}$. Γ^n is expected to be coarse where the solution is smooth, and refined in regions of sharp variations. For the solution to evolve from U_a^n into U_a^{n+1}, three basic steps are undertaken.

1) **Refinement:** $U_a^{n+} \leftarrow \mathcal{E}U_a^n$.
2) **Evolution:** $\bar{U}_a^{n+1} \leftarrow \mathcal{L}_a U_a^{n+}$.
3) **Coarsening:** $U_a^{n+1} \leftarrow \mathcal{T}_\varepsilon \bar{U}_a^{n+1}$.

Refinement is a preemptive processes to prevent possible movement or steepness of the solution between time steps. Since the regions of smoothness or irregularities of the solution may change with time, Γ^n may not be convenient anymore at the next time step $t = t^{n+1}$. Therefore, before doing the time evolution, the representation of the solution should be extended to a grid Γ^{n+}, which is expected to contain Γ^n and Γ^{n+1} as well. Then, a time evolution operator $\mathcal{L}_a$ is applied. The subscript a means that spatial derivatives at points $\nu \in \Gamma^{n+}$ are performed by means of uniform finite differences, using step size proportional to the point local scale. Finally, a thresholding operation $\mathcal{T}_\epsilon$ (coarsening) is applied, in order to eliminate from Γ^{n+} those points that are unnecessary for an accurate representation of U_a^{n+1}.

TABLE I
STABILITY PARAMETERS

	$p=1$	$p=2$	$p=3$	$p=4$
K_β^{-1}	2.0	1.4575	1.2713	1.1697
K_α^{-1}	1.0	0.75	0.6844	0.6585

Therefore, in the SPR method the numerical solution is represented in sparse grids dynamically adapted to the solution. The grid updating is performed by two operators: refinement and coarsening. In both cases, the interpolating subdivision scheme plays a crucial role. In the coarsening, it is the basic tool for the definition of the wavelet coefficients which are used as local regularity indicators. In the refinement, it is used to predict the solution at new points added to the grid. It is also used in the computations of the adapted finite differences, when some required stencil points are not in Γ^{n+}. For details of such procedures, we refer to [8] and [9].

III. FD Schemes for Maxwell's Equations

For the applications of the present paper, we shall consider the unidimensional set of Maxwell's equations, corresponding to a plane wave propagating in the x direction

$$\frac{\partial H_y}{\partial t} = \frac{1}{\mu}\frac{\partial E_z}{\partial x}, \quad \frac{\partial E_z}{\partial t} = \frac{1}{\epsilon}\frac{\partial H_y}{\partial x}$$

where E_z and H_y are the electrical and magnetic fields, ϵ is the electrical permittivity, and μ is the magnetic permeability. To simplify the notation, H_y will be denoted by H and E_z will be denoted by E.

A. Schemes for Staggered Grids

As in the classic FDTD scheme, we use Yee's mesh for the field discretizations

$$E_k^n \approx E_z(k\Delta x, n\Delta t),$$
$$H_{k+\frac{1}{2}}^{n+\frac{1}{2}} \approx H_y\left(\left(k+\frac{1}{2}\right)\Delta x, \left(n+\frac{1}{2}\right)\Delta t\right)$$

and we shall consider FD schemes of the form

$$H_{k+1/2}^{n+1/2} = H_{k+1/2}^{n-1/2} + \frac{\Delta t}{\mu \Delta x}\sum_m E_m^n \alpha(k-m) \quad (1)$$

$$E_k^{n+1} = E_k^n + \frac{\Delta t}{\epsilon \Delta x}\sum_m H_{m+1/2}^{n+1/2}\alpha(k-m-1) \quad (2)$$

where the coefficients are supposed to satisfy $\alpha(-k) = -\alpha(k-1)$.

B. Schemes for Nonstaggered Grids

Now, both fields are discretized in the same uniform grid

$$E_k^n \approx E_z(k\Delta x, n\Delta t), \quad H_k^n \approx H_y(k\Delta x, n\Delta t)$$

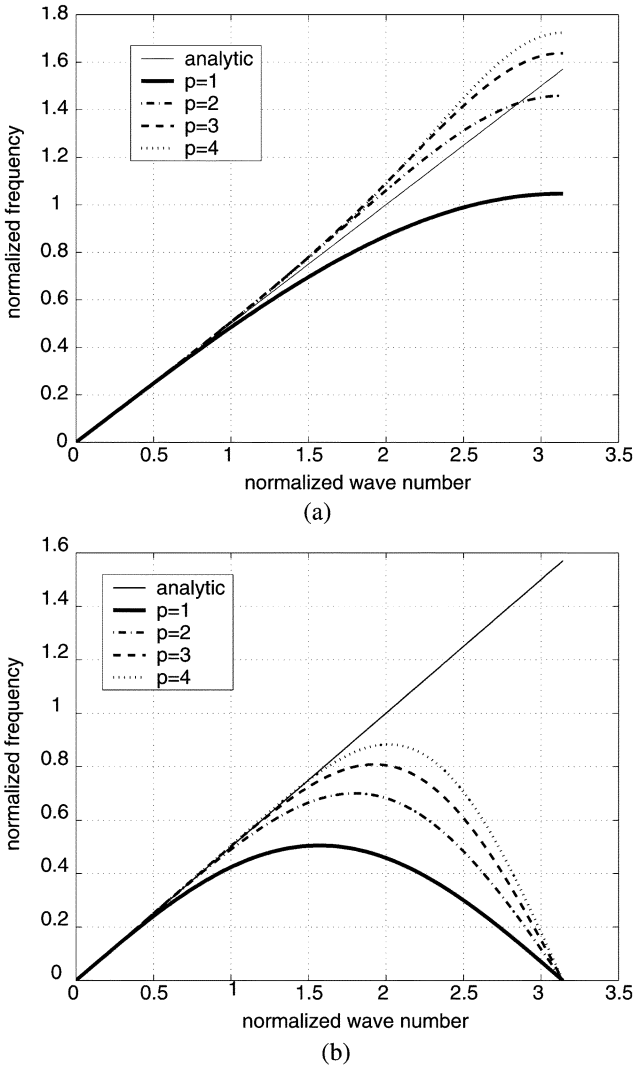

Fig. 2. Numerical dispersion for staggered (top) and nonstaggered grids (bottom): Normalized frequency versus normalized wave number S, for CFL $s = 0.5$ and different orders p. (a) Staggered grid. (b) Nonstaggered grid.

and we shall consider FD schemes of the form

$$H_k^{n+1} = H_k^n + \frac{\Delta t}{\mu \Delta x} \sum_m E_m^n \beta(k-m) \tag{3}$$

$$E_k^{n+1} = E_k^n + \frac{\Delta t}{\epsilon \Delta x} \sum_m H_m^{n+1} \beta(k-m) \tag{4}$$

where the coefficients are supposed to satisfy $\beta(k) = -\beta(k)$.

IV. Stability and Numerical Dispersion

Let us consider plane wave solutions in the form $H_y(x,t) = He^{i(\kappa x - \omega t)}$ and $E_z(x,t) = Ee^{i(\kappa x - \omega t)}$, where ω is the frequency in time and κ is the wave number in space. Replacing these expressions in the Maxwell's system of equations, the conclusion is that plane waves solutions are admissible if the analytical dispersion relation holds $\omega^2 \mu \epsilon = \kappa^2$.

Schemes for Staggered Grids: Plane wave solutions exist for these schemes provided that the numerical dispersion relation holds

$$\sin^2\left(\frac{\Omega}{2}\right) = s^2[(\tilde{\alpha}(S))^2]$$

where $\tilde{\alpha}(\eta) = \sum_{k \geq 0} \alpha(k) \sin((k+1/2)\eta)$, $\Omega = \omega \Delta t$ is the normalized frequency, $S = \kappa \Delta x$ is the normalized wave number, and $s = (c\Delta t)/(\Delta x)$ is the CFL parameter. Consequently, the stability condition reads $s \leq (1)/(K_\alpha)$, for $K_\alpha = \max_\eta |\tilde{\alpha}(\eta)|$.

Schemes for Nonstaggered Grids: Analogously, plane wave solutions exist for these schemes provided that the numerical dispersion relation holds

$$\sin^2\left(\frac{\Omega}{2}\right) = s^2[(\tilde{\beta}(S))^2]$$

where $\tilde{\beta}(\eta) = \sum_{k \geq 1} \beta(k) \sin(k\eta)$. Now, the stability condition reads $s \leq (1)/(K_\beta)$, for $K_\beta = \max_\eta |\beta(\eta)|$.

A. Examples

To analyze the gridding effect in the two classes of FD schemes with respect to numerical dispersion and stability, we shall consider some particular cases of FD schemes of orders $2p$, $2 \leq p \leq 4$. As described in the Appendix, they can be formulated as collocation schemes in approximation spaces spanned by the translations and dilations of a basic interpolating scaling function $\Phi(x)$ chosen in the family of scaling functions of Delauriers–Dubuc [13]. The coefficients are given in Tables III and Table IV. For comparison, we shall also consider second order schemes ($p = 1$). For staggered grids, the coefficients are $\alpha(-1) = 1, \alpha(0) = -1$ and $\alpha(k) = 0$ otherwise, which corresponds to the FDTD scheme. For nonstaggered grids, we consider $\beta(1) = -\beta(-1) = -1/2$ and $\beta(k) = 0$, otherwise. For these two low-order schemes, the dispersion relations read

$$\sin^2\left(\frac{\Omega}{2}\right) = s^2 \sin^2\left(\frac{S}{2}\right),$$

$$\sin^2\left(\frac{\Omega}{2}\right) = s^2 \frac{\sin^2(S)}{4}$$

which corresponds to the S-MRTD versions of the Haar formulations II and I, respectively, described in [14].

Fig. 1 (top) shows the curves for $|\tilde{\alpha}(S)|, 0 \leq S \leq \pi$, for different consistency orders. We note that $K_\alpha = K_\alpha(p)$ occurs at $z = \pi$ and such value increases with p. This means that CFL numbers are smaller for higher orders schemes in staggered grids. Similarly, consider now the plots in Fig. 1 (bottom) corresponding to $|\tilde{\beta}(S)|, 0 \leq S \leq \pi$, for different orders. Note that $K_\beta = K_\beta(p)$ also increases with p. However, these values are smaller than in the case of staggered grids. This implies that the CFL parameters K_β^{-1} for the explicit scheme in nonstaggered grids are greater than K_α^{-1}. These parameters are listed in Table I for different values of p.

Fig. 2 depicts the numerical dispersion curves for the schemes in staggered grids (top) and nonstaggered grids (bottom) for the value of the CFL parameter $s = 0.5$. For comparison, the linear analytic dispersion curve $\Omega = sS$ is also plotted. For both grids, we note the improvement in accuracy for low wave numbers S, as p increases. However, for nonstaggered grids, the errors are significant for large wave numbers S, while in the case of staggered grids these differences are less significant for higher orders p.

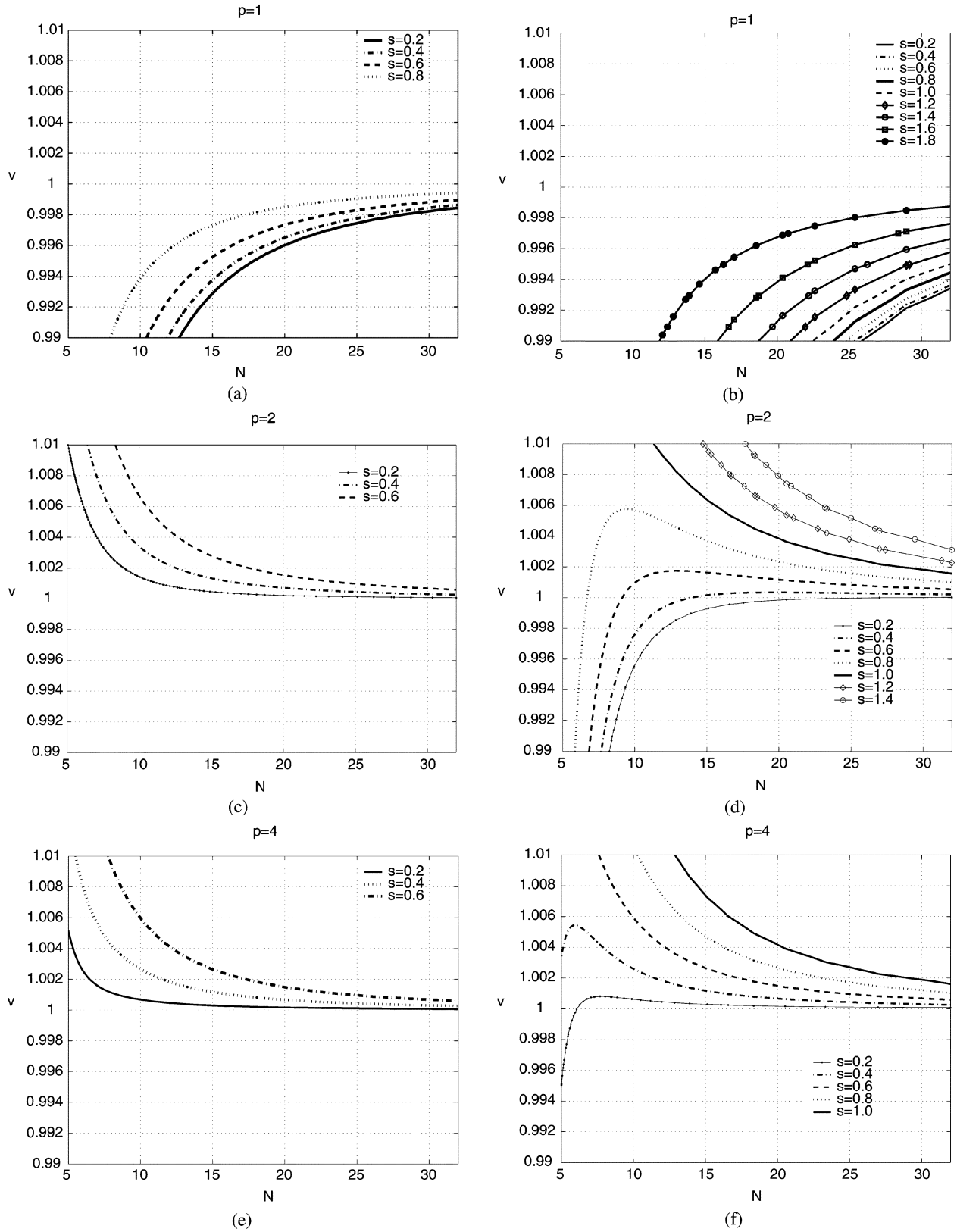

Fig. 3. Dispersion analysis: Plots of the normalized velocity $\bar{v}$ versus the number of cells per wavelength N, for several values of the CFL parameter s. Left: staggered grids. Right: nonstaggered grids.

The Effect of the CFL Parameter: For a fixed CFL parameter, the analysis of the previous section indicates that staggered grids seem to be preferable from the dispersion view point. However, we have seen that the stability region for the schemes in nonstaggered grids is wider than in staggered grids. Therefore, a comparison of the accuracy of the two kinds of schemes should

also take into account the effect of the CFL parameter in the numerical dispersion. For this purpose, we consider the normalized velocity $\bar{v} = v_p/c$, where $v_p = \omega/\kappa$, and $c = (1)/(\sqrt{\epsilon\mu})$. Define $\delta = \Delta x\omega/c2\pi$. Note that, if $\lambda = cT$ is the wavelength, where $T = 2\pi/\omega$ is the period, then for $\delta = 1/N, N = \lambda/h$ is the number of cells per wavelength. This means that δ measures the relative grid density. Using these variables, the analytical dispersion relation reads $\bar{v} = 1$, and the numerical dispersion relations become

$$\sin(s\pi\delta) = s\tilde{\alpha}\left(\frac{2\pi\delta}{\bar{v}}\right)$$

$$\sin(s\pi\delta) = s\tilde{\beta}\left(\frac{2\pi\delta}{\bar{v}}\right)$$

for staggered and nonstaggered grids, respectively. Since now the analytical dispersion does not depend on the CFL parameter, this new way of representing the dispersion relations facilitates the analysis of the effect of this parameter on the accuracy of the different methods, and shown in Fig. 3. Note that the plots for FD schemes in staggered and nonstaggered grids have different CFL parameters, which are taken within the stability range of each scheme. For the case of staggered grids, the plots of $\bar{v}$ as a function of the number of cells per wavelength are shown in Fig. 3 (left), for some CFL numbers varying within the stability range $s \leq (1)/(K_\alpha(p))$. As expected, these plots show that the efficiency increases with the order of the scheme. For instance, with CFL $= 0.6$, more than 10 cells per wavelength are necessary to get an accuracy close to 99% using the FDTD method $(p = 1)$, while the higher order schemes require less than 8 cells per wavelength to get the same accuracy. Furthermore, these plots also show that using the FDTD method the dispersion curves approaches the constant analytic value $\bar{v} = 1$, from the bottom up, as s approaches the CFL stability limit $s = 1$. For $p > 1$, the tendency is in the opposite direction, from the top down, and as s tends to zero. For the models in nonstaggered grids, Fig. 3 (right) shows the plots of $\bar{v}$ as a function of the number of cells per wavelength, with CFL parameters varying within the stability range $s \leq (1)/(K_\beta(p))$. We also note that for $p = 1$, the dispersion curves approaches the constant analytic value $\bar{v} = 1$, as s approaches the CFL stability limit $s = 2$, and for $p > 1$, there is a tendency in the opposite direction in certain ranges of s and N. As expected, the efficiency also increases with the other. It follows from these plots that staggering the grids may be helpful, especially for low-order schemes and grid densities. However, as the grid density and order of accuracy increase, the effect is less noticeable.

Since the schemes in nonstaggered grids allow a wider stability range, the efficiency of these two FD schemes cannot be evaluated for a fixed CFL parameter, and a more accurate analysis requires taking into account the effects of the CFL number and grid density. For the fourth-order FD scheme, we present in Fig. 4 the numerical dispersion curves in the plane $N \times S$, within their stability limits, for two levels of accuracy: $\bar{v} = 1.01$ (1% of accuracy) and $\bar{v} = 1.001$ (0.1% of accuracy). Note that, for each given level of accuracy, the curve of the nonstaggered grid scheme is above the curve of the staggered grid scheme. This means that, for the same grid density, the CFL parameter (and so Δt) for the nonstaggered grid scheme can be greater than in the staggered case, a computational advantage.

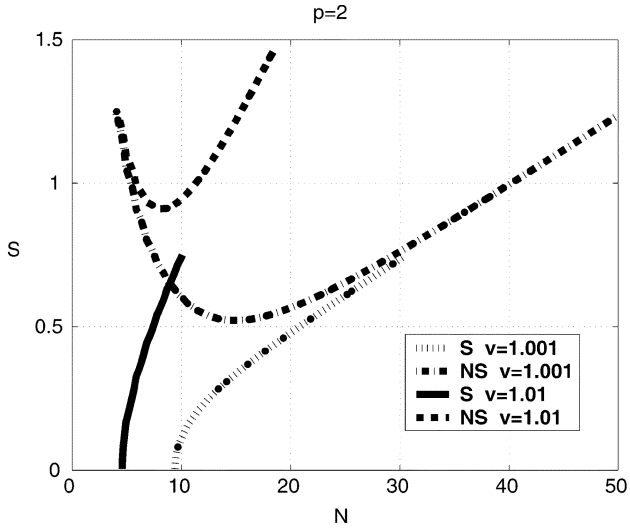

Fig. 4. Dispersion analysis: Plots of the normalized wave number S versus the number of cells per wavelength N, for two levels of accuracy, in the staggered and nonstaggered cases.

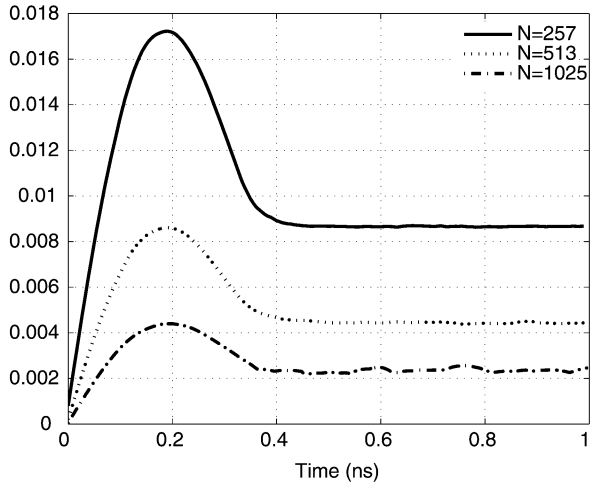

Fig. 5. Each curve depicts the evolution in time of the maximum absolute difference between the solutions for the electric field, obtained using the staggered and nonstaggered schemes, for CFL $s = 0.5$. The maximum value of the electric field was normalized to unity. Note that N, in this case, is the number of samples of the finest grid.

V. SPR Numerical Simulations

Our purpose in the present section is to analyze the performance of the SPR method for the numerical solution of Maxwell's equations. In the operational part of the SPR method we could have chosen any accurate and stable finite difference scheme. For the applications of this section, we use two reference finite difference schemes described in Section III, namely, the schemes on staggered and nonstaggered grids obtained by collocation in shift invariant approximating spaces, spanned by the Delauriers–Dubuc scaling functions associated with cubic interpolation $(p = 2)$.

In order to compare the schemes in the staggered and nonstaggered grids, we consider an example in 1-D where the fields at $t = 0$ are assumed to be $E_z(x, 0) = e^{-150(x-1/2)^2}$ and $H_y(x, 0) = 0, 0 \leq x \leq 1$. The usual absorbing PML regions are placed close to the artificial boundaries.

First, in Fig. 5, we plot the maximum absolute value of the difference between the numerical solutions for the electric

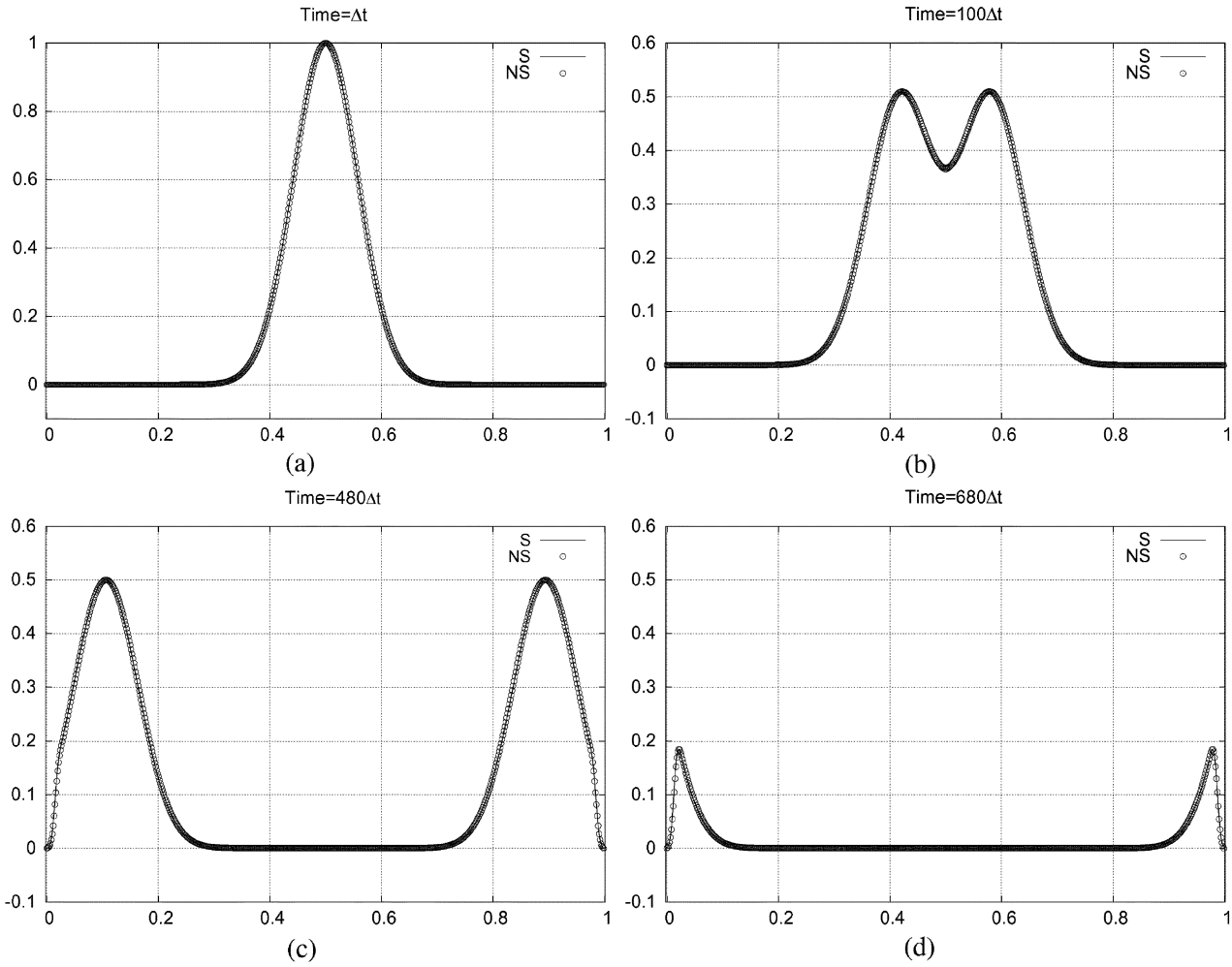

Fig. 6. Evolution of the electrical field for the staggered and nonstaggered grid schemes.

field, using staggered and nonstaggered uniform grids, and $\mathrm{CFL} = 0.5$. The amplitude of the electric field was normalized to unity. We observe that, as the grid density increases, both solutions tend to coincide, confirming the theoretical evidence of Fig. 2, since smaller values of s correspond to a larger number of points.

The results in Fig. 6 are for the simulations of the SPR schemes for staggered and nonstaggered grids after 100, 480, and 680 time steps. We have used a threshold $\varepsilon_E = 10^{-6}$ for the electric field and $\varepsilon_H = 10^{-9}$ for the magnetic field. The coarsest grid has 20 points and 5 levels of refinement are allowed. At each point of the sparse computational grid, we apply the finite differences with step size of the finest local scale resolution and the time step is chosen for stability at this scale level. We can see that the solutions obtained with both schemes are quite similar, and no spurious oscillations were detected, contrarily to [12].

The curves in Fig. 7 describe the evolution of the number of grid points in the adaptive grids for the electrical field expressed as a percentage of the total number of points in the uniform grid of the finest scale level. For this example, we also observed that allowing more than 5 scale levels does not significantly affect the number of points in the adaptive grids.

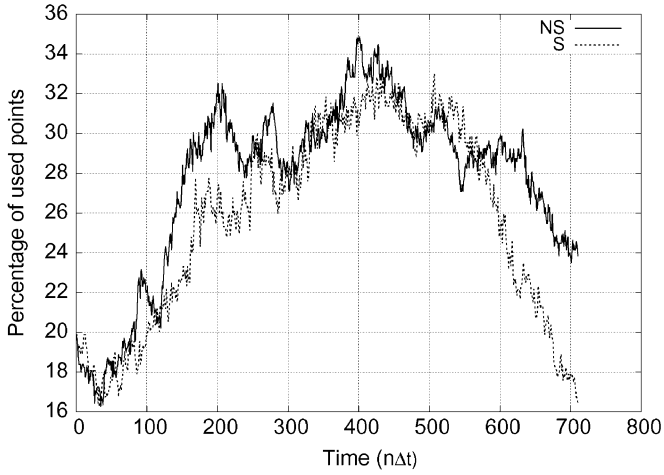

Fig. 7. Evolution of the percentage of grid points with time, for the electrical field, and staggered and nonstaggered grids.

The plots in Fig. 8 show the normalized computational effort W versus the maximum absolute error in the electrical field at $t = 0.75$ ns, between the reference solution and the SPR solutions. All the SPR solutions have the same number of points

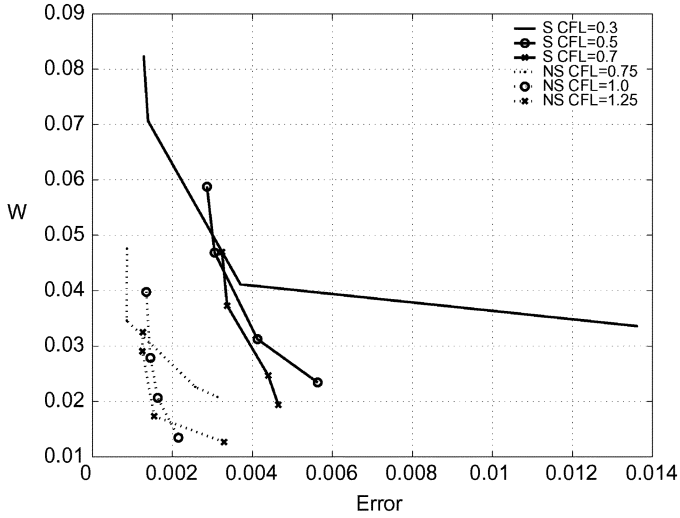

Fig. 8. Computational effort W (divided by the effort required by FDTD, $\mathrm{CFL} = 1$) versus maximum absolute error, for several values of the CFL parameter, in the staggered and nonstaggered cases.

in the finest grid and 6 levels of refinement are allowed. All the SPR curves were plotted using four points corresponding to four different values of the threshold ($5\times10^{-8}, 10^{-7}, 5\times10^{-7}$, and 10^{-6}). The computational effort W is defined as the product of the number of required time steps with the average number of points in the adaptive grids. As expected, the errors increase with decreasing computational effort, in all cases.

The plots show that, for a given accuracy, less computational effort is required with the adaptive scheme in nonstaggered grids than with the scheme in staggered grids, confirming the theoretical evidence of Fig. 5.

VI. Concluding Remarks

This paper compared in detail two classes of high-order SPR schemes for Maxwell equations. We considered implementations of the operational part by FD schemes on staggered grids in the time-space domain for the magnetic and electric field components. In addition to these, we also considered implementations in which the grids coincide for both fields. The following points follow from our analysis and numerical simulations.

- For stability reasons, there are limitations in explicit schemes in the choice of the time-step, defined by the CFL condition. The stability region decreases for increasing approximation orders, and it is less restrictive for nonstaggered grids than for staggered ones.
- From the viewpoint of numerical dispersion, staggering the grids is helpful, specially for low-order schemes and grid densities. However, as the grid density and order of accuracy increase, the effect becomes less noticeable.
- To correctly compare the accuracy with respect to the type of grid, it is important to take into accuracy the effect of the CFL. More precisely, it is important to evaluate and compare the CFL numbers required for the schemes to achieve a prescribed accuracy level with a certain number of cells per wavelength. With respect to this, we observed that higher order schemes in nonstaggered grids can be used with larger CFL parameters.
- The use of nonstaggered grids facilitates the implementation of adaptive strategies.
- As a result of the combination of these factors, the schemes based on nonstaggered grids require less computational effort to achieve a certain accuracy.

We conclude that high-order FD schemes in nonstaggered grids have a good potential to be used in SPR adaptive simulations of Maxwell equations in higher dimensions.

Appendix

A. Interpolating Multiresolution Analyses

In a multiscale framework, functions are represented in different scale levels, and the main tools are appropriate transformations relating the information at the finest scale level j to the lower ones, and vice versa. In the context of interpolating multiresolution analyses, the input data f^j contains the sample values at a grid in finest scale level. After a transformation T^j, the output contains the information f^0 in the coarsest level, and d^ℓ that keeps the details between a scale level ℓ and the next upper level $\ell+1$. Schematically, we have

$$f^j \overset{T^j}{\to} f^j_{MR} = (f^0, d^0 \dots d^{j-1}).$$

In a uniform setting, each scale level ℓ corresponds to a uniform grid X^ℓ. Starting from X^0, the grid at the coarsest level with spacing Δx^0, a hierarchy of uniform grids $X^\ell, \ell \geq 1$, with spacing $\Delta x^\ell = \Delta x^0 2^{-\ell}$, are obtained by dyadic refinement. This means that, if x^ℓ_k are the points in X^ℓ, then $X^{\ell+1}$ is formed by the old points $x^{\ell+1}_{2k} = x^\ell_k$ and new midpoints $x^{\ell+1}_{2k+1} = (x^\ell_k + x^\ell_{k+1})/(2)$. In the applications of the present paper, the grid points in X^ℓ may be of the form $x^\ell_k = k\Delta x^\ell$ or $x^\ell_k = (k+(1)/(2))\Delta x^\ell$. In a nonuniform setting, the principle is also to have the information data hierarchically organized by different levels of resolution. On this matter, we are concerned with a sequence of embedded grids $\Gamma^\ell \subset \Gamma^{\ell+1}$. It shall be assumed that $\Gamma^0 = X^0$, and $\Gamma^\ell \subset X^\ell$, for $\ell > 0$, is constructed from $\Gamma^{\ell-1}$ by including some new points of $X^\ell \setminus X^{\ell-1}$.

As described in the following algorithms, for the definition of T^j and its inverse $(T^j)^{-1}$, the main ingredients are reconstruction interpolating operators $I^\ell f(x)$ that predict $f(x)$ at any location x from the knowledge of its discrete sample values f^ℓ at Γ^ℓ. The wavelet coefficients d^ℓ_ν are defined for points $\nu \in \Gamma^{\ell+1} \setminus \Gamma^\ell$ as the errors in this prediction.

Analysis—$f^j \overset{T^j}{\to} (f^0, d^0, \dots d^{j-1})$:

- *For* $\ell = j-1, \dots, 0$ *Define* $f^\ell_\nu = f^j_\nu$ *if* $\nu \in \Gamma^\ell$ *If* $\nu \in \Gamma^{\ell+1} \setminus \Gamma^\ell$, *calculate* $\tilde{f}^{\ell+1}_\nu = I^\ell f(\nu)$, *and set* $d^\ell_\nu = f^{\ell+1}_\nu - \tilde{f}^{\ell+1}_\nu$.

Synthesis—$(f^0, d^0, \dots, d^{j-1}) \overset{(T^j)^{-1}}{\to} f^j$:

- *For* $\ell = 0, \dots, j-1$ *Define* $f^{\ell+1}_\nu = f^\ell_\nu$ *if* $\nu \in \Gamma^\ell$ *If* $\nu \in \Gamma^{\ell+1} \setminus \Gamma^\ell$, *calculate* $\tilde{f}^{\ell+1}_\nu = I^\ell f(\nu)$ *and set* $f^{\ell+1}_\nu = d^\ell_\nu + \tilde{f}^{\ell+1}_\nu$.

For uniform grids X^ℓ, the definition of the interpolation operator $I^\ell f(x)$ uses the classical interpolation subdivision scheme, which is done interactively. On the first step, we set $I^\ell f(x^\ell_k) = f(x^\ell_k)$. Having $I^\ell f(x^m_k) = s^m_k$ being defined for all $x^m_k \in X^m, m \geq \ell$, then the definition is extended to X^{m+1} by means of a prediction interpolation scheme P^{m+1}_m. For other nondyadic points, the definition is set by density arguments, as in the classical subdivision scheme.

For nonuniform grids, the definition of the interpolation operator $I^\ell f(x)$ uses a simple modification of the classical in-

TABLE II
COEFFICIENTS $h(k), k \geq 1$

k	$p=1$	$p=2$	$p=3$	$p=4$
1	$\frac{1}{4}$	$\frac{9}{32}$	$\frac{150}{512}$	$\frac{1225}{4086}$
3		$-\frac{1}{32}$	$-\frac{25}{512}$	$-\frac{245}{4086}$
5			$\frac{3}{512}$	$\frac{49}{4086}$
7				$-\frac{5}{4086}$

terpolation subdivision scheme [15]. On the first step, we set $I^\ell f(x_k^0) = f(x_k^0)$. For $0 \leq m < \ell$, having $I^\ell f(x_k^m) = s_k^m$ being defined for all $x_k^m \in X^m$, then the definition is extended to $X^{m+1} \setminus \Gamma^\ell$ by means of a prediction interpolation scheme P_m^{m+1}, and it is set $I^\ell f(x_k^{m+1}) = f(x_k^{m+1})$, if $x_k^{m+1} \in \Gamma^\ell \cap X^{m+1}$. For other points, the definition is set as in the classical subdivision scheme.

The main ingredient to perform this task is a prediction interpolating operator $P_m^{m+1} : s^m \to s^{m+1}$, where $s^m = (s_k^m)$ and $s^{m+1} = (s_k^{\ell m+1})$ are sequences labeled by the points $x_k^m \in X^m$ and $x_k^{m+1} \in X^{m+1}$, respectively. In the applications of the present paper, the following interpolating prediction scheme is adopted, using central polynomial Lagrange interpolation of degree $M-1$, where $M = 2p$ is an even integer.

- At the old points x_{2k}^{m+1}, define $s_k^{m+1} = s_k^m$.
- At the new points x_{2k+1}^{m+1}, use the interpolating polynomial of degree $M-1$ based on the M samples of s^m closest to this position, and set s_{2k+1}^{m+1} equal to the value of this interpolating polynomial at x_{2k+1}^{m+1}.

In the case of uniform grid $\Gamma^j = X^j$, the interpolation operator can be represented in the form

$$I^j f(x) = \sum_k f_k^j \Phi_k^j(x)$$

where $\Phi_k^j(x) = \Phi((1)/(\Delta x^j)(x - x_k^j))$ and the basic function $\Phi = \Phi_M$ is the scaling function of Delauriers-Dubuc [13]. It is defined iteratively, by means of the subdivision scheme. Starting from its values at the integers $\Phi(k) = \delta_{0k}$, then the values of $\Phi(x)$ at the dyadic grid points $x = k2^{-\ell}$ at level ℓ are obtained from its values at level $\ell - 1$ using the prediction interpolating scheme, as described above. Therefore, $\Phi(x) = 2\sum_n h(n)\Phi(2x - n)$, where $h(n)$ are the coefficients associated to the central Lagrange polynomial interpolation of degree $M-1$. These coefficients are symmetric $h(-k) = h(k), h(0) = 1/2$, and vanish for even integers $k \neq 0$ and all integers such that $|k| \geq 2p + 1$. The values for $h(k), k \geq 1$ are presented in Table II, for $1 \leq p \leq 4$. For $p = 1, \Phi(x)$ is the hat function with support in $[-1, 1]$. For $p > 1$, there is no explicit formula for $\Phi(x)$, but it can be proved that $\Phi \in C^1$ is a symmetric function, $\Phi(-x) = \Phi(x)$, vanishing for $|x| \geq 2p - 1$. Furthermore, its regularity increases with p [13]. Defining $\psi_k^\ell(x) = \Phi_{2k+1}^{\ell+1}(x)$, it can be proved that the multilevel transformations T^j and $(T^j)^{-1}$ amount to change from the one level basis $\{\Phi_k^j(x)\}$ to the multilevel basis $\{\Phi_k^{j_0}(x)\} \cup \bigcup_{\ell=j_0}^{j-1}\{\psi_k^\ell(x)\}$ and vice versa.

TABLE III
NONZERO COEFFICIENTS $\alpha(k), k \geq 0$

k	$p=2$	$p=3$	$p=4$
0	-1.22916667	-1.29181	-1.31103404
2	0.093750	0.137134	0.156010071
3	-0.010416667	-0.0287618	-0.041995746
4		0.00347014	0.008654324
5		-8.02654×10^{-6}	-0.000830869
6			-0.000010899
7			0.000000004

TABLE IV
NONZERO COEFFICIENTS $\beta(k), k > 0$

k	$p=2$	$p=3$	$p=4$
1	-2/3	-272/365	-1747/2203
2	1/12	53/365	1483/7724
3		-16/1095	-3999/11882
4		-1/2920	73/32823
5			128/743295
6			-1/1189272

B. SPR Representation

As described in the previous section, given the input data f^j formed by function values in a grid $\Gamma^j \subset X^j$, after the application of the wavelet transform T^j, this discrete information is organized by levels of resolution as $f_{MR}^j = (f^0, d^0 \ldots d^{j-1})$. At each level l, the wavelet coefficients d^l are defined in terms of local interpolation errors at the new points of the current level of discretization. In the construction of the adapted grids, the idea is to use the wavelet coefficients as indicators of local smoothness of the solution. This is the main ingredient in the definition of the thresholding operator $\mathcal{T}_\varepsilon$: only those points in Γ^j corresponding to wavelet coefficients of magnitude greater than ε should be kept in the adapted grid Γ_ε^j. This procedure led to sparse representations $f_{\mathrm{SPR},\varepsilon}^j$ where only the sample values required to reconstruct f^j with error less than ε are retained.

C. Collocation Methodology

In this section, we explain how the two sets of FD schemes introduced in Section III can be obtained using the collocation methodology in approximating spaces spanned by the translates and dilates of the basic interpolating function $\Phi(x)$. First, for

nonstaggered grids, we consider sample values for the components of both fields E and H at the same uniform grid in space and time

$$E_k^n = E(k\Delta x, n\Delta t),$$
$$H_k^n = H(k\Delta x, n\Delta t).$$

Based on these discrete values, approximations $IE(x, n\Delta t)$, for the components of E, and $IH(x, n\Delta t)$, for the components of H, are defined at any point x by

$$IE(x, n\Delta t) = \sum_k E_k^n \Phi\left(\frac{x}{\Delta x} - k\right)$$
$$IH(x, n\Delta t) = \sum_k H_k^n \Phi\left(\frac{x}{\Delta x} - k\right).$$

Collocating the spatial derivatives of these interpolation operators at the grid points, and integrating in time using a first order Euler scheme, we obtain the set of discrete equations (3)–(4), where $\beta(k) = \Phi'(k)$.

We now use the staggered Yee's mesh for the discretization, as in the classic FDTD scheme, which corresponds to the following samples of the components of H and E:

$$E_k^n = E(k\Delta x, n\Delta t)$$
$$H_{k+\frac{1}{2}}^{n+\frac{1}{2}} = H\left(\left(k+\frac{1}{2}\right)\Delta x, \left(n+\frac{1}{2}\right)\Delta t\right).$$

Based on these discrete values, interpolating approximation schemes for the components of H and E are defined in terms of the translations and dilations of the basic function $\Phi(x)$

$$IE(x, n\Delta t) = \sum_k E_k^n \Phi\left(\frac{x}{\Delta x} - k\right)$$
$$IH(x, \left(n+\frac{1}{2}\right)\Delta t) = \sum_k H_{k+\frac{1}{2}}^{n+\frac{1}{2}} \Phi\left(\frac{x}{\Delta x} - k - \frac{1}{2}\right).$$

As in the previous case, collocating the spatial derivatives at the Yee's grid points, and integrating in time using a first-order Euler scheme, we obtain the set of discrete equations (1)–(2), where $\alpha(k) = \Phi'(k + (1)/(2))$. If the $\Phi(x)$ is an interpolating scaling function, and the refinement equation is differentiated in both sides, it follows that the coefficients $\beta(k)$ can be obtained as the solution of the eigenvalue problem $\beta(k) = 4\sum_{k'} h(k')\beta(2k - k')$, after the normalization relation $\sum_k k\beta(k) = 1$. Because of the symmetry of $\Phi(x)$, we obtain $\beta(-k) = -\beta(-k)$. The symmetry of $\Phi(x)$ also implies that $\alpha(-k) = -\alpha(k-1)$. Using the scaling relation, these coefficients can be obtained from $\beta(k)$ by the formula $\alpha(k) = 4\sum_n h(n)\beta(2k+1-n)$. The coefficients are given in Table III, for staggered grids, and Table IV, for nonstaggered grids. It can be proved that these FD schemes can also be interpreted as Galerkin S-MRTD discretizations in terms of Daubechies scaling functions φ_p of approximation order p, as described in [16].

ACKNOWLEDGMENT

The research of this paper is part of a scientific international cooperation between GRICES (Portugal) and CAPES (Brazil). This research has also been supported in part by CNPq and FAPESP (Brazil) and FCT (Portugal).

REFERENCES

[1] A. Taflove, *Computational Electrodynamics: The Finite-Difference Time-Domain Method*. Norwood, MA: Artech House, 1996.
[2] Q. X. Chu and H. Ding, "Second-order accurate FDTD equations at magnetic media interfaces," *IEEE Trans. Magn.*, vol. 42, no. 10, pp. 3141–3143, Oct. 2006.
[3] S. Y. Yang, S. L. Ho, P. H. Ni, and G. Z. Ni, "A combined wavelet-FE method for transient, electromagnetic-field computations," *IEEE Trans. Magn.*, vol. 42, no. 4, pp. 571–574, Apr. 2006.
[4] A. Geranmayeh, R. Moini, S. H. H. Sadeghi, and A. Deihimi, "A fast wavelet-based moment method for solving thin-wire EFIE," *IEEE Trans. Magn.*, vol. 42, no. 4, pp. 575–578, Apr. 2006.
[5] P. Alotto, A. De Cian, and G. Molinari, "A time-domain 3-D full-Maxwell solver based on the cell method," *IEEE Trans. Magn.*, vol. 42, no. 4, pp. 799–802, Apr. 2006.
[6] ——, *Advances in Computational Electrodynamics: The Finite-Difference Time Domain Method*. Norwood, MA: Artech House, 1998.
[7] M. Krumpholtz and L. B. Katehi, "MRTD: New time-domain schemes based on multiresolution analysis," *IEEE Trans. Microw. Theory Tech.*, vol. 44, no. 4, pp. 555–571, Apr. 1996.
[8] M. Holmstrom, "Wavelet based methods for time dependent PDEs," Ph.D. dissertation, Uppsala Univ., Uppsala, Sweden, 1997.
[9] ——, "Solving hyperbolic PDEs using interpolating wavelets," *SIAM J. Sci. Comput.*, vol. 21, no. 2, pp. 405–420, 1999.
[10] P. Pinho, P. J. Ferreira, S. M. Gomes, and J. R. Pereira, "Solving Maxwell's equations using interpolating wavelets," in *Proc. 5th Conf. Telecommunications*, C. Salema, Ed. *et al.*, 2005.
[11] P. Pinho, "Resolução das equações de Maxwell por análise de multiresolução usando wavelets interpolatórias," Ph.D. dissertation, Univ. Aveiro, Aveiro, Portugal, 2004.
[12] G. Rubinacci, A. Tamburrino, S. Ventre, and F. Villone, "Interpolating wavelets for the solution of Maxwell equations in the time domain," *IEEE Trans. Magn.*, vol. 34, no. 5, pp. 2775–2778, Sep. 1998.
[13] G. Delauriers and S. Dubuc, "Symmetric iterative interpolation processes," *Construct. Approx.*, vol. 5, pp. 49–68, 1986.
[14] C. D. Sarris and L. P. B. Katehi, "Fundamental gridding-related dispersion effects in multiresolution time-domain schemes," *IEEE Trans. Microw. Theory Tech.*, vol. 49, no. 12, pp. 2248–2257, Dec. 2001.
[15] F. Plantevin, "Wavelets on irregular meshes," *Adv. Comput. Math.*, vol. 4, no. 1, pp. 293–329, Dec. 1995.
[16] M. C. Cunha and S. M. Gomes, "The relation between Petrov-Galerkin and collocation methods using spline multiresolution analyses," *Revista de la Unión Matemática Argentina*, vol. 41, no. 1, pp. 61–78, 1998.

Manuscript received July 7, 2006; revised November 29, 2006. Corresponding author: P. Pinho (e-mail: ppinho@deetc.isel.ipl.pt).